Limits on axion-like particles from Mrk 421 with 4.5-year period observations by ARGO-YBJ and *Fermi*-LAT

Hai-Jun Li,[1, 2] Jun-Guang Guo,[1, 2] Xiao-Jun Bi,[1, 2] Su-Jie Lin,[3, 1] and Peng-Fei Yin[1]

[1]*Key Laboratory of Particle Astrophysics, Institute of High Energy Physics,*
Chinese Academy of Sciences, Beijing 100049, China
[2]*School of Physics, University of Chinese Academy of Sciences, Beijing 100049, China*
[3]*School of Physics and Astronomy, Sun Yat-Sen University, Zhuhai 519082, GuangDong, China*
(Dated: January 7, 2022)

In this work, we investigate the axion-like particle (ALP)-photon oscillation effect in the spectra of the blazar Markarian 421 (Mrk 421) using 4.5 years of the Astrophysical Radiation with Ground-based Observatory at YangBaJing (ARGO-YBJ) and *Fermi* Large Area Telescope (*Fermi*-LAT) data. These data are collected during the common operation time, which cover ten activity phases of Mrk 421. No significant ALP-photon oscillation effect is confirmed. On the other hand, not all the observations of the ten phases can be individually used to set the 95% confidence level (C.L.) constraint on the ALP parameter space. However, the constraint can be significantly improved if the analyses for the ten phases are combined. We find that the upper limit at 95% C.L. on the ALP-photon coupling $g_{a\gamma}$ set by the ARGO-YBJ and *Fermi*-LAT observations of Mrk 421 is within $\sim [2 \times 10^{-11},\ 6 \times 10^{-11}]\,\mathrm{GeV}^{-1}$ for the ALP mass of $\sim 5 \times 10^{-10}\,\mathrm{eV} \lesssim m_a \lesssim 5 \times 10^{-7}\,\mathrm{eV}$.

I. INTRODUCTION

In order to solve the strong *CP* problem in Quantum chromodynamics (QCD), Peccei and Quinn proposed a new $U(1)$ symmetry in 1977 [1, 2]. Soon thereafter, the existence of the axion under this symmetry was recognized independently by Weinberg [3] and Wilczek [4]. The QCD axion can be described as the pseudo Nambu-Goldstone boson of a spontaneously broken $U(1)_{\mathrm{PQ}}$ symmetry [5]. Apart from the canonical QCD axion, various axion-like particles (ALPs) have also been proposed in the new physics model beyond the standard model, such as string theory [6–8]. The axion-like particle (ALP) mass m_a and the coupling constant with photons $g_{a\gamma}$ are taken to be two independent parameters in the research. This is different from the scenario of the QCD axion, where these two parameters are related to each other. If ALPs are produced non-thermally in the early Universe, they may account for all or a significant fraction of the cold dark matter [9–13].

ALPs could be detected through their coupling to photons in the magnetic field in the laboratory [14–16], such as CAST [17, 18], PVLAS [19, 20], OSQAR [21, 22], and ABRACADABRA [23, 24]. The coupling between the ALP and photons would also lead to ALP-photon oscillation for the photons ejecting from the high energy γ-ray sources which are far from the Earth and would modify their γ-ray energy spectra [16]. This effect could lead to the observable modifications in the γ-ray telescopes [25, 26]. Many works have been performed to study this effect for many astrophysical sources and set constraints on the ALP parameter space [25–51].

In this work, we focus on the very high energy (VHE) γ-ray observations of the blazar Markarian 421 (Mrk 421), which is one of the most widely studied and brightest sources in the extragalactic TeV sky with the redshift of $z_0 = 0.031$. It was firstly detected at VHE by the Whipple Observatory in 1992 [52] and has been well detected with many imaging atmospheric Cherenkov telescopes [53–60]. Mrk 421 is classified as a high synchrotron-peaked BL Lac object and is a very active blazar with major outbursts [61], which are composed of many short flares in both the X-ray and γ-ray regions.

Thanks to the results of Astrophysical Radiation with Ground-based Observatory at YangBaJing (ARGO-YBJ) [58, 59] and *Fermi* Large Area Telescope (*Fermi*-LAT) [57], the high energy component of the spectral energy distribution of Mrk 421 has been completely covered in the γ-ray band from 0.1 GeV to 10 TeV. Ref. [59] reported the 4.5-year multi-wavelength data recorded from August 2008 to February 2013. This period contains the ten steady and flaring phases of Mrk 421. In this work, we consider the effect of the ALP-photon oscillation in the high energy γ-ray spectra of Mrk 421 with these ten phases and combine the results of all the phases together to set constraint on the ALP parameter space.

This paper is organized as follows. In Section II, we introduce the propagation of high energy γ-ray with the ALP-photon oscillation in three parts, including the source region, the extragalactic space, and the Milky Way region. In Section III, we describe the observation data of Mrk 421 by ARGO-YBJ and *Fermi*-LAT in the common operation time used in this work. In Section IV, we introduce the data fitting and statistical methods. In Section V, we give the constraints on the ALP parameter space from the Mrk 421 observations. The conclusion is given in Section VI.

II. PROPAGATION OF THE ALP-PHOTON SYSTEM

The ALP-photon oscillation effect occurring in the magnetic field would modify the γ-ray energy spectra of astrophysical sources, which are far from the Earth

[25, 26]. The ALP-photon coupling is described by the following Lagrangian [16]

$$\mathcal{L}_{a\gamma} = -\frac{1}{4} g_{a\gamma} a F_{\mu\nu} \tilde{F}^{\mu\nu} = g_{a\gamma} a \mathbf{E} \cdot \mathbf{B}, \qquad (1)$$

where $g_{a\gamma}$ is the coupling constant, a is the ALP field, $F_{\mu\nu}$ is the electromagnetic field tensor, $\tilde{F}^{\mu\nu}$ is the dual tensor, and $\mathbf{E}$ and $\mathbf{B}$ are the electric and magnetic fields, respectively. The ALP and photon are interconvertible in the external magnetic field and could be described by the ALP-photon beam [29]

$$\Psi = (A_1, A_2, a)^T, \qquad (2)$$

where A_1 and A_2 represent the photon transverse polarization states in the directions of x_1 and x_2 which are perpendicular to the propagation direction x_3, respectively.

The density matrix of the ALP-photon system is given by

$$\rho = \Psi \otimes \Psi^\dagger. \qquad (3)$$

After oscillation in numerous consecutive domains, the final density matrix of the ALP-photon system is

$$\rho(s) = T(s)\rho(0)T^\dagger(s), \qquad (4)$$

where $T(s)$ is the whole transfer matrix for the propagation distance s. The initial beam state $\rho(0)$ is assumed to be

$$\rho(0) = \frac{1}{2}\text{diag}(1,1,0). \qquad (5)$$

The final survival probability of the photon in the ALP-photon system is given by [29]

$$P_{\gamma\gamma} = \text{Tr}\left((\rho_{11} + \rho_{22})T(s)\rho(0)T^\dagger(s)\right), \qquad (6)$$

with

$$\rho(s)_{11} = \text{diag}(1,0,0), \quad \rho(s)_{22} = \text{diag}(0,1,0). \qquad (7)$$

The ALP-photon conversion would become maximal and energy-independent in the strong mixing regime $E_{\text{crit}} \lesssim E \lesssim E_{\text{max}}$ with [33, 37]

$$E_{\text{crit}} = \frac{|m_a^2 - \omega_{\text{pl}}^2|}{2g_{a\gamma}B} \qquad (8)$$
$$\simeq 2.5 \text{ GeV } |m_{\text{neV}}^2 - 1.4 \times 10^{-3} \ n_{\text{cm}^{-3}}|g_{11}^{-1}B_{\mu\text{G}}^{-1},$$

and

$$E_{\text{max}} = \frac{90\pi}{7\alpha}\frac{B_{\text{cr}}^2 g_{a\gamma}}{B} \simeq 2.12 \times 10^6 \text{ GeV } g_{11}B_{\mu\text{G}}^{-1}, \qquad (9)$$

where m_a is the ALP mass, $\omega_{\text{pl}} \sim \sqrt{4\pi\alpha n_e/m_e}$ is the plasma frequency, B is the external magnetic field, n_e is the electron density, α is the fine-structure constant, and $B_{\text{cr}} = m_e^2/|e| \sim 4.41 \times 10^{13}$ G is the critical magnetic field. In the above equations, we have used the notations $m_{\text{neV}} \equiv m_a/1$ neV, $n_{\text{cm}^{-3}} \equiv n_e/1$ cm^{-3}, $g_{11} \equiv g_{a\gamma}/10^{-11}$ GeV^{-1}, and $B_{\mu\text{G}} \equiv B/1$ μG.

In order to obtain the transfer matrix for the ALP-photon system, the propagation process of the system is divided into three parts, including the propagations in the source region, the extragalactic space, and the Milky Way region [25, 26].

TABLE I. The benchmark values of the parameters for the BJMF model in the ten phases of Mrk 421.

Phase	B_0(G)	δ_{D}	$n_0(10^3 \text{ cm}^{-3})$
S1	0.048	38	1.919
S2	0.17	15	3.009
OB	0.054	35	2.228
F1	0.14	10	0.269
F2	0.092	17	0.825
F3	0.080	41	1.544
F4	0.033	35	3.527
F5	0.072	31	2.296
F6	0.085	15	8.809
F7	0.115	30	1.963

Firstly, we neglect the internal γ-ray absorption and the ALP-photon oscillation within the broad line region of the source, and only consider the ALP-photon oscillation effect in the blazar jet magnetic field (BJMF). Following Refs. [31, 39], here the BJMF of Mrk 421 is considered as the BL Lac type with the transverse magnetic field $B_{\text{jet}}(r)$ and the electron density $n_{\text{el}}(r)$ profiles. The radial profile of the magnetic field strength is [62–64]

$$B_{\text{jet}}(r) = B_0 \left(\frac{r}{r_{\text{VHE}}}\right)^{-1}, \qquad (10)$$

where r_{VHE} is the distance of the VHE emission site to the central black hole and B_0 is the magnetic field strength at r_{VHE}. The modified model for the electron density distribution is [65]

$$n_{\text{el}}(r) = n_0 \left(\frac{r}{r_{\text{VHE}}}\right)^{-2}, \qquad (11)$$

where n_0 is the electron density at r_{VHE}. These equations hold in the co-moving frame of the blazar jet. The photon energy E_j in this frame is related to the energy E_L in the laboratory frame with the transformation $E_j = E_L/\delta_{\text{D}}$, where δ_{D} is the Doppler factor. In the region with $r > 1$ kpc, the strength of BJMF is set to be zero. More details about this BJMF model can be found in Refs. [31, 39].

In principle, the parameters for the BJMF model can be derived from the fit to the data using the synchrotron self-Compton model. The best-fit values of B_0 and δ_{D} in the ten phase of Mrk 421 given by Ref. [59] are listed in Table I. The electron distribution within the emitting plasma is assumed to be a broken power law in Ref. [59]. Using the best-fit values of the energy normalization u_e and the first index of the broken power law p_1, we derive the benchmark values of n_0 listed in Table I.

It is difficult to derive the precise value of $r_{\rm VHE}$ from the observations. $r_{\rm VHE}$ can be roughly estimated as $r_{\rm VHE} \sim R_{\rm VHE}/\theta_{\rm jet}$, where $R_{\rm VHE}$ is the radius of the VHE emitting plasma blob and $\theta_{\rm jet}$ is the angle between the jet axis and the line of sight. In the analysis of ARGO-YBJ $R_{\rm VHE}$ for all the phases are arbitrarily set to be 10^{16} cm, while no $\theta_{\rm jet}$ is provided in Ref. [59]. The fit using a multiple-flare model leads to $\theta_{\rm jet} \in [0.38° - 1.8°]$ in Ref. [66], which is consistent with $\theta_{\rm jet} = 1.3°$ derived in Ref. [67]. In Ref. [68], the values of $R_{\rm VHE}$ and $\theta_{\rm jet}$ of Mrk 421 are found to be 6×10^{15}cm and $2.0°$, respectively. Using these values, we find $r_{\rm VHE} \sim \mathcal{O}(10^{17}) - \mathcal{O}(10^{18})$ cm. In the following analysis, we shall take $r_{\rm VHE} = 10^{17}$ cm as the benchmark parameter for all the phases.

After leaving the jet, the ALP-photon system enters the host galaxy. Following Refs. [30, 39], we do not consider the ALP-photon oscillation effect in the magnetic field of the host galaxy since it is too small. In general, the blazar may be located at a rich cluster, where the turbulent inter-cluster magnetic field is about $\mathcal{O}(1)$ μG [69–71]. We find that the ALP-photon oscillation could be significant in this magnetic field. However, there is no evidence that Mrk 421 is reside in such a rich environment. Therefore, we do not consider the ALP-photon oscillation effect in the inter-cluster magnetic field.

The upper limit of the extragalactic magnetic field on the largest cosmological scale is $\mathcal{O}(1)$ nG [72]. Its actual value is not clear and would be much lower than this upper limit [42, 73]. In this work, we do not consider the effect of this magnetic field for the ALP-photon system propagation in the extragalactic space and only focus on the attenuation effect induced by the extragalactic background light (EBL) due to the pair production process $\gamma + \gamma_{\rm BG} \rightarrow e^+ + e^-$. This attenuation effect can be characterized by the factor of $e^{-\tau}$ with the optical depth [28, 74]

$$\tau = c \int_0^{z_0} \frac{\mathrm{d}z}{(1+z)H(z)} \int_{E_{\rm th}}^{\infty} \mathrm{d}\omega \frac{\mathrm{d}n(z)}{\mathrm{d}\omega} \bar{\sigma}\left(E_\gamma, \omega, z\right), (12)$$

where z_0 is the redshift of the source, $H(z)$ is the rate of the Hubble expansion, $E_{\rm th}$ is the threshold energy, $\bar{\sigma}$ is the integral cross section of the pair production, E_γ and ω are the source and background photon energies, respectively, and $\mathrm{d}n/\mathrm{d}\omega$ is the proper number density of the EBL. The EBL model used here is taken from Ref. [74] and is shown in Fig. 1.

For the propagation of the ALP-photon system in the Milky Way region, we consider the ALP-photon oscillation effect in the Galactic magnetic field. Here we neglect the random component on the small scale and take the regular component of the Galactic magnetic field on the large scale from Ref. [80].
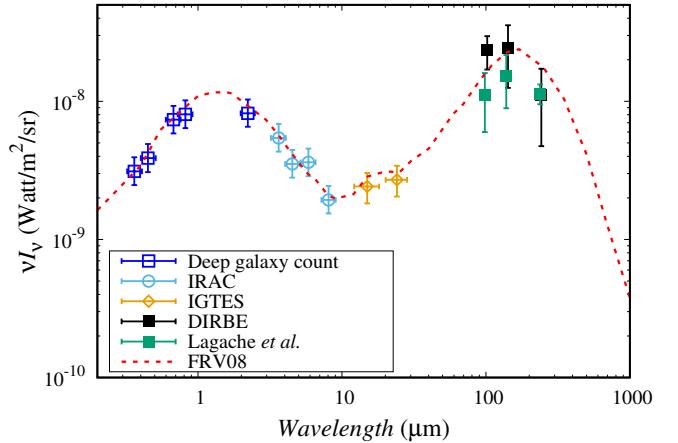

FIG. 1. The cosmic infrared background spectrum (dashed line) from the multi-wavelength reference model with the galaxy evolution effect named FRV08 model in Ref. [74]. The observed data from Refs. [75–79] are also shown.

III. GAMMA-RAY DATA OF MRK 421 FROM ARGO-YBJ AND *FERMI*-LAT

The ARGO-YBJ [81] detector, located at Yangbajing Cosmic Ray Observatory (Tibet, P.R. China, 90.5° East, 30.1° North), is an air shower array exploiting the full coverage approach at very high altitude, with the aim of studying the VHE γ-ray astronomy and cosmic-ray physics.

In Ref. [59], the ARGO-YBJ collaboration reported the spectral variation of Mrk 421 at different wavebands and divided the whole observation period into ten phases according to the large X-ray and GeV γ-ray flares. The γ-ray spectra of Mrk 421 at lower energies in the common operation time from *Fermi*-LAT [82] are also analysed in Ref. [59]. The analysis is performed with the standard ScienceTool and the corresponding threads provided by *Fermi*-LAT.

The ten phases of the ARGO-YBJ observation for Mrk 421 [59] are described as follows. Mrk 421 showed a low activity at all wavebands from August 2008 to June 2009. This is marked as Steady 1 (S1) phase. Then the source entered a long lasted outburst phase from June 2009 to June 2010, which is denoted as Outburst (OB) phase. During this active phase, three large flares Flare 1 (F1), Flare 2 (F2), and Flare 3 (F3) were clearly detected. After May 2010, Mrk 421 entered a low steady phase until October 6. This phase lasted about one month and is marked as Flare 4 (F4) phase.

Then Mrk 421 came to a long and steady phase (S2) from November 2010 to June 2012, which lasted about 1.6 years. The embedded strong flare denoted as Flare 5 (F5) phase, which occurred in September 2011 and lasted 7 days, has been separated from the phase S2. In the whole year of 2012, the flux of γ-ray measured by ARGO-YBJ [83] and *Fermi*-LAT [84] reached a high level from

2012 July 9 to September 17. Two peaks are marked as Flare 6 (F6, from 2012 July 9 to 21) phase and Flare 7 (F7, from 2012 July 22 to September 16) phase.

IV. DATA FITTING AND STATISTICAL METHODS

In order to fit the experimental data of ARGO-YBJ and *Fermi*-LAT under the null hypothesis, the form of the intrinsic energy spectrum of Mrk 421 is taken to be a super-exponential cut-off power law (SEPWL)

$$\Phi_{\text{int}}(E) = F_0 \left(\frac{E}{E_0}\right)^{-\Gamma} \exp\left(-\left(\frac{E}{E_c}\right)^d\right), \quad (13)$$

where E_0 is taken to be 1 GeV, F_0, Γ, E_c, and d are treated as free parameters. We also test other forms of the intrinsic spectrum including the exponential cut-off power law and the logarithmic parabola function. We find that the best-fit χ^2 under the null hypothesis of the SEPWL is the smallest.

Considering the modification of the energy spectrum induced by the ALP, the expected γ-ray energy spectrum under the ALP hypothesis is determined by the survival probability of the photon $P_{\gamma\gamma}$ in Eq. (6)

$$\Phi_{\text{w ALP}}(E) = P_{\gamma\gamma}\Phi_{\text{int}}(E), \quad (14)$$

with the intrinsic energy spectrum $\Phi_{\text{int}}(E)$.

We also take into account the energy resolution of the experiments in the analysis. The energy resolutions of ARGO-YBJ and *Fermi*-LAT are adopted to be 13% [85] and 15% [1], respectively. Considering the energy dispersion function $D(E', E_1, E_2)$ where E' is the actual energy, the expected γ-ray flux at the detector in the energy bin between E_1 and E_2 can be derived as [50]

$$\Phi' = \frac{\int_0^\infty D(E', E_1, E_2)\Phi(E')\,\mathrm{d}E'}{E_2 - E_1}, \quad (15)$$

where $\Phi(E')$ is the γ-ray spectrum before detection. The χ^2 value is given by

$$\chi^2 = \sum_{i=1}^{N} \frac{(\Phi'_i - \tilde{\phi}_i)^2}{\delta_i^2}, \quad (16)$$

where N is the point number, Φ'_i is the expected γ-ray flux, $\tilde{\phi}_i$ is the observed flux, and δ_i is the corresponding uncertainty of the observation.

In order to set the constraint on the ALP parameter space, we define the threshold value χ^2_{th} as

$$\chi^2_{\text{th}} = \chi^2_{\text{min}} + \Delta\chi^2, \quad (17)$$

———————

with the minimum best-fit χ^2_{min} in the $m_a - g_{a\gamma}$ plane and the $\Delta\chi^2$ corresponding to the particular confidence level (C.L.). Due to the non-linear dependence of the spectral irregularities on the ALP parameters, we derive the value of $\Delta\chi^2$ from the Monte Carlo simulation [49].

We generate 400 sets of the observed γ-ray spectra of Mrk 421 in the pseudo-experiments that are realized by Gaussian samplings [43]. For each set of the simulated spectrum, we can derive the best-fit χ^2 for both the null hypothesis $\widehat{\chi}^2_{\text{null}}$ and the ALP hypothesis $\widehat{\chi}^2_{\text{w ALP}}$. For each Monte Carlo data set, we have the test statistic (TS) value

$$\text{TS} = \widehat{\chi}^2_{\text{null}} - \widehat{\chi}^2_{\text{w ALP}}. \quad (18)$$

Then we obtain the TS distribution under the null hypothesis for all data sets that obeys the non-central χ^2 distribution. The $\Delta\chi^2$ corresponding to the certain confidence level can be derived from the TS distribution with the effective degree of freedom (d.o.f.) and the non-centrality λ. Finally, we assume that the probability distribution under the alternative hypothesis with ALP is approximated with the distribution under the null hypothesis and use the value of $\Delta\chi^2$ derived above to set the constraint on the ALP parameter space [49].

TABLE II. The best-fit values of $\chi^2_{\text{w/o ALP}}$ in the ten phases under the null hypothesis.

Phase	data point number	$\chi^2_{\text{w/o ALP}}$
S1	16	18.88
S2	16	9.47
OB	16	18.38
F1	7	1.45
F2	9	0.99
F3	9	6.61
F4	11	3.91
F5	7	7.18
F6	11	7.88
F7	15	5.20

V. RESULTS

In this section, we set constraints on the ALP parameter space using the data of ARGO-YBJ and *Fermi*-LAT in the ten phases of Mrk 421. The best-fit values of $\chi^2_{\text{w/o ALP}}$ under the null hypothesis are listed in Table II. The reduced χ^2 under the null hypothesis in the ten phases are around the average value 1.04. Only the reduced χ^2 in the phase F5 is large as 2.39. In Fig. 2, we also give the best-fit γ-ray spectra for the phases of S1, S2, OB, and F7 under the null and ALP hypotheses. We can see that the null hypothesis can well fit the ARGO-YBJ and *Fermi*-LAT data.
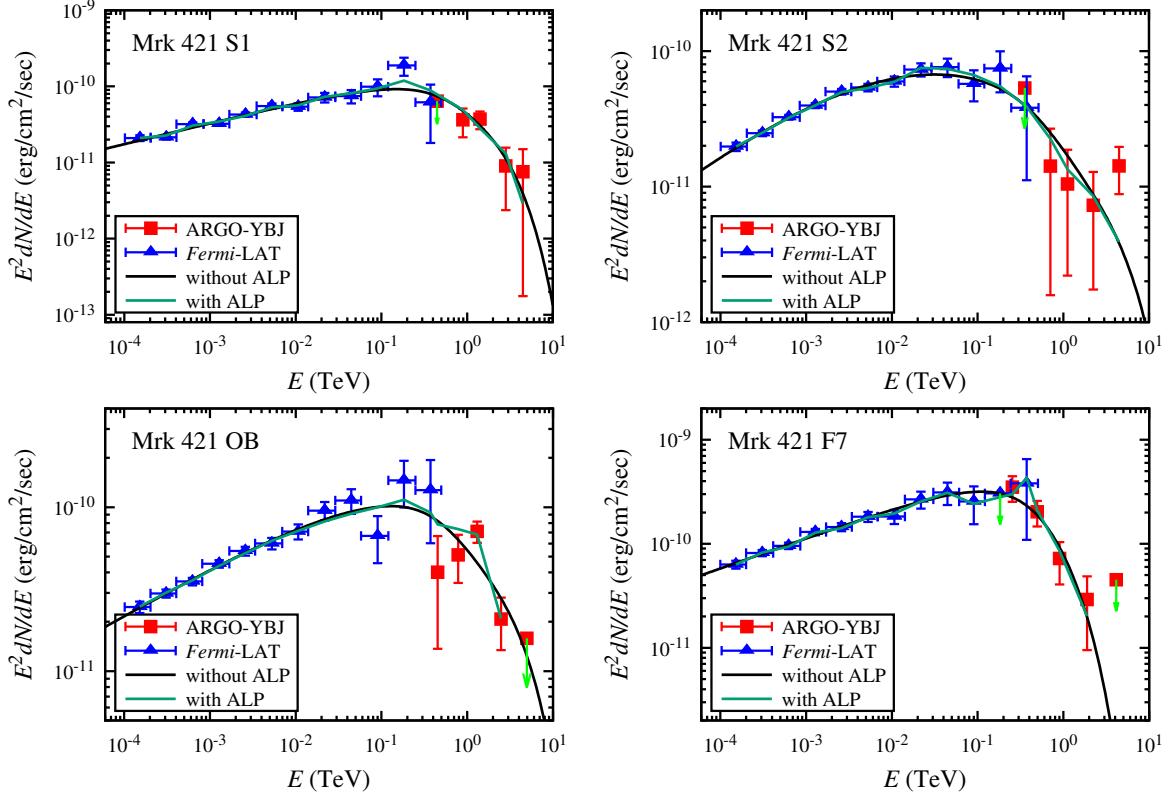
FIG. 2. The best-fit γ-ray spectra of Mrk 421 in the phases S1 (top left), S2 (top right), OB (bottom left), and F7 (bottom right). The black lines represent the spectra under the null hypothesis with $\chi^2_{\text{w/o ALP}} = 18.88$, 9.47, 18.38, and 5.20 in the four phases. The green lines represent the spectra under the ALP hypothesis with $\chi^2_{\min} = 11.81$, 6.49, 12.85, and 2.57 in the four phases. The parameters for the BJMF model are given by Table I. The experimental data are from ARGO-YBJ and $Fermi$-LAT [59].

FIG. 3. The distributions of $\chi^2_{\text{w ALP}}$ in the $m_a - g_{a\gamma}$ plane for the ten phases of Mrk 421. The parameters for the BJMF model are given by Table I. The red contours represent the excluded regions at 95% C.L. in the phases S1, S2, OB, F3, F4, F6, and F7. The horizontal line represents the upper bound on $g_{a\gamma}$ set by CAST [18] of $g_{a\gamma} < 6.6 \times 10^{-11}$ GeV^{-1}.
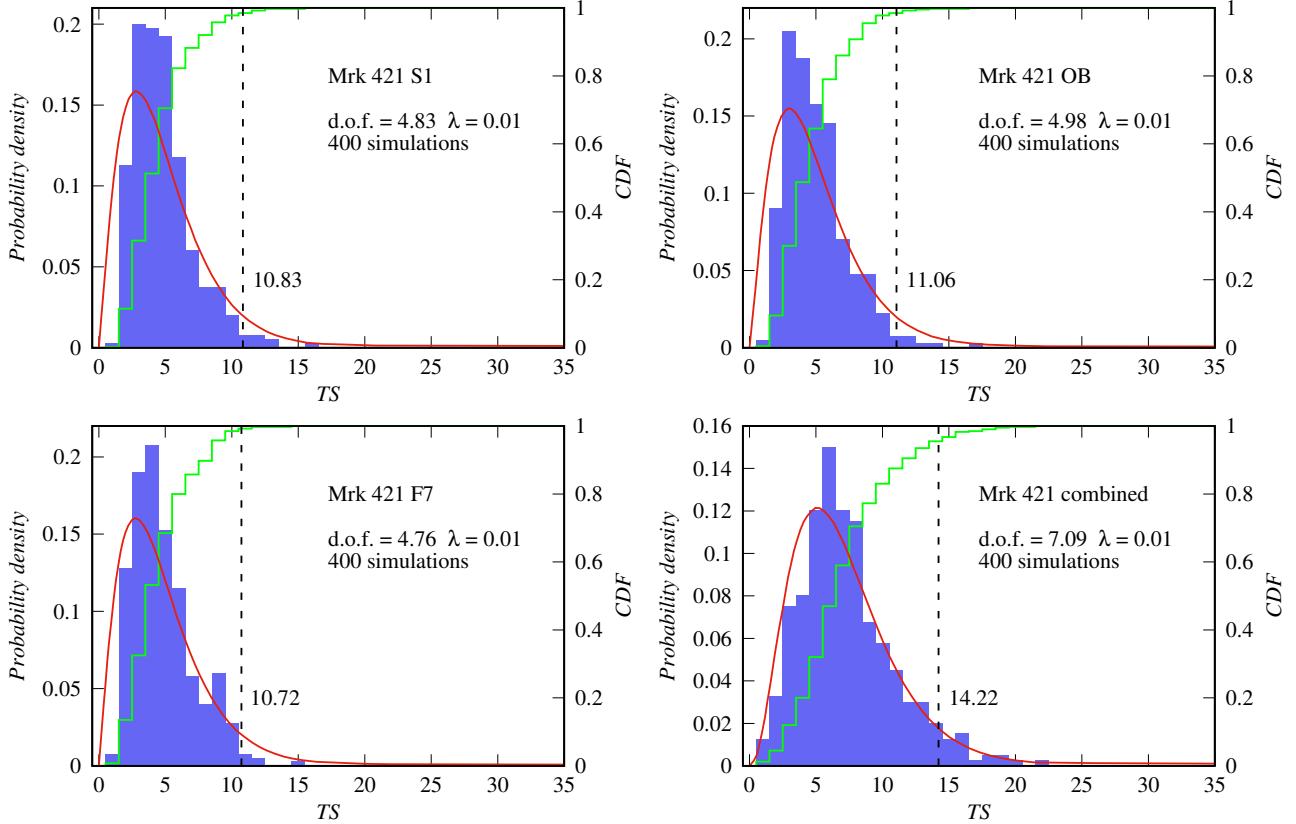
FIG. 4. The TS distributions of the phase S1 (top left), OB (top right), F7 (bottom left), and the combined phases (bottom right) with the BJMF parameters given by Table I. The red lines represent the fitted non-central χ^2 distributions. The green lines represent the CDF of the TS distributions.
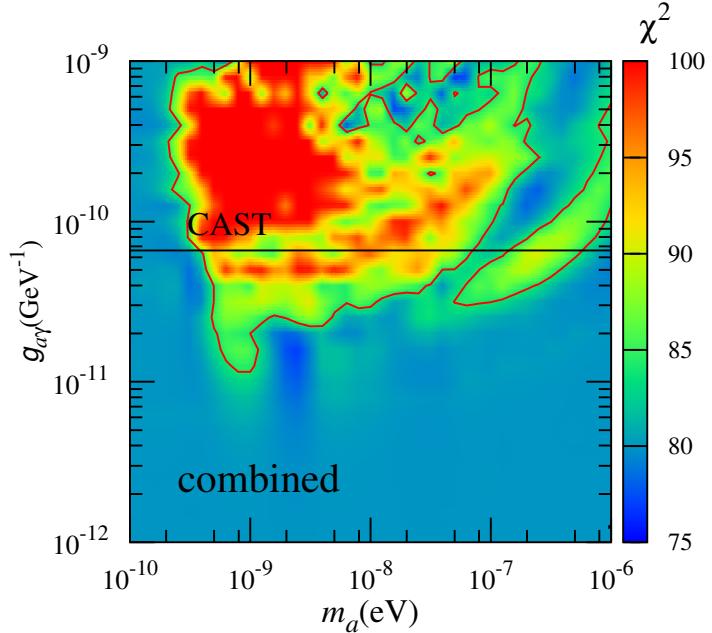

FIG. 5. The $\chi^2_{\text{w ALP}}$ distribution of the combined phases with the BJMF parameters given by Table I. The red contour represents the excluded region at 95% C.L.

TABLE III. The minimum best-fit values of $\chi^2_{\min}$ in the ten phases under the ALP hypothesis. The effective d.o.f. of the TS distributions and the values of $\Delta\chi^2$ corresponding to 95% C.L. are also listed. The combined results for the ten phases are also shown. The values of the BJMF parameters are given by Table I.

Phase	$\chi^2_{\min}$	effective d.o.f.	$\Delta\chi^2$
S1	11.81	4.83	10.83
S2	6.49	4.86	11.88
OB	12.85	4.98	11.06
F1	0.77	1.59	5.20
F2	0.49	3.03	7.89
F3	2.94	3.03	7.89
F4	2.27	1.16	4.26
F5	5.45	1.17	4.28
F6	4.79	1.16	4.26
F7	2.57	4.76	10.72
combined	72.39	7.09	14.22

The distributions of $\chi^2_{\text{w ALP}}$ under the ALP hypothesis in the ten phases are shown in Fig. 3 with the benchmark values of the BJMF parameters. The minimum best-fit values of $\chi^2_{\min}$ in the $m_a - g_{a\gamma}$ plane for the ten phases are listed in Table III.

Then we can derive the TS distributions for the ten phases. We find that the non-centralities of all the TS distributions are about 0.01. The effective d.o.f. of the distributions and the threshold values of $\Delta\chi^2$ corresponding to 95% C.L. are listed in Table III. In Fig. 4, we plot the TS distributions for the phases S1, OB, and F7. The red lines represent the fitted non-central χ^2 distributions with the effective d.o.f. of 4.83, 4.98, and 4.76 for the phases S1, OB, and F7, respectively. The green lines represent the cumulative distribution functions (CDF) of the TS distributions. Using these functions, we can derive the values of $\Delta\chi^2$ corresponding to the 95% C.L. threshold as 10.83, 11.06, and 10.72 for the phases S1, OB, and F7, respectively.

With the values of $\Delta\chi^2$ for all the phases, the constraints on the ALP parameter space at 95% C.L. are shown in Fig. 3. It can be seen that the data sets of the ten phases set very different constraints. Using the data of the phases S1, S2, OB, F6, and F7, we could find some explicit excluded parameter regions at 95% C.L. For the other phases, the 95% C.L. constraint cannot be significantly set in the $m_a - g_{a\gamma}$ plane. This is because that the observations in these phases provide too few data points.

In order to make a reliable implication, we combined the results in the ten phases together. The TS distribution and the combined $\chi^2_{\text{w ALP}}$ distribution in the $m_a - g_{a\gamma}$ plane are shown in Fig. 4 and 5, respectively. The red contour in Fig. 5 represents the upper limit at 95% C.L. Compared with the limit set by CAST [18] about $g_{a\gamma} < 6.6 \times 10^{-11}$ GeV^{-1}, the upper
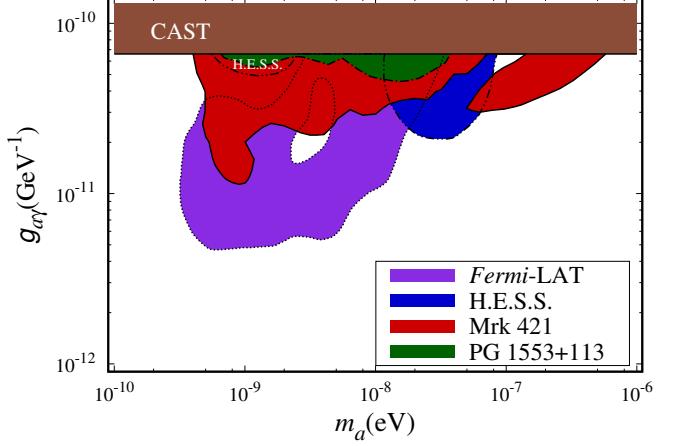

FIG. 6. The excluded regions at 95% C.L. set by the Mrk 421 observations of ARGO-YBJ and *Fermi*-LAT. The red contour represents the result derived with the BJMF parameters given by Table I. For comparison, the constraints set by CAST [18], the PKS 2155-304 observation of H.E.S.S. [48], and the NGC 1275 observation of *Fermi*-LAT [49] are shown. We also show the constraint set by the PG 1553+113 observations using the data from H.E.S.S. II and *Fermi*-LAT [50].

limit on the ALP-photon coupling $g_{a\gamma}$ set by the ARGO-YBJ and *Fermi*-LAT observations of Mrk 421 is within $\sim [2 \times 10^{-11}, \ 6 \times 10^{-11}]$ GeV^{-1} for the ALP mass of $\sim 5 \times 10^{-10}$ eV $\lesssim m_a \lesssim 5 \times 10^{-7}$ eV.

For comparison, we also show the constraints from the PKS 2155-304 observation of H.E.S.S. [48] and the NGC 1275 observation of *Fermi*-LAT [49] in Fig. 6. The combined limit from the Mrk 421 observations obtained here extends the excluded region to $g_{a\gamma} \gtrsim 3 \times 10^{-11}$ GeV^{-1} for $\sim 5 \times 10^{-10}$ eV $\lesssim m_a \lesssim 2 \times 10^{-9}$ eV and a part region for $m_a \simeq 2 \times 10^{-7}$ eV below the CAST limit. This constraint is also stricter than that derived from the observation data of PG 1553+113 [50].

Finally, we discuss the impact of the uncertainties of the BJMF parameters. The combined constraints on the ALP parameter space for different values of the BJMF parameters B_0, δ_D, n_0, and r_{VHE} are calculated. In each panel of Fig. 7, we only change the values of one parameter as listed in Table IV and take the other parameters as the benchmark values. For the minimal (maximal) cases of B_0 and δ_D with the uncertainties given by Ref. [59], we take the 1σ minimal (maximal) values of the parameters in all the ten phases and calculate the corresponding constraints. For the minimal (maximal) case of n_0, the values of n_0 listed in Table IV are calculated using the 1σ minimal (maximal) values of u_e and p_1 given by Ref. [59]. It can be seen that the constraints would become stringent for large B_0, while the changes of the other parameters do not significantly affect the results.

In Fig. 8, we also show the impact of r_{VHE} on the final result. Since there is no direct way to derive the precise value of r_{VHE}, the uncertainty of this value would

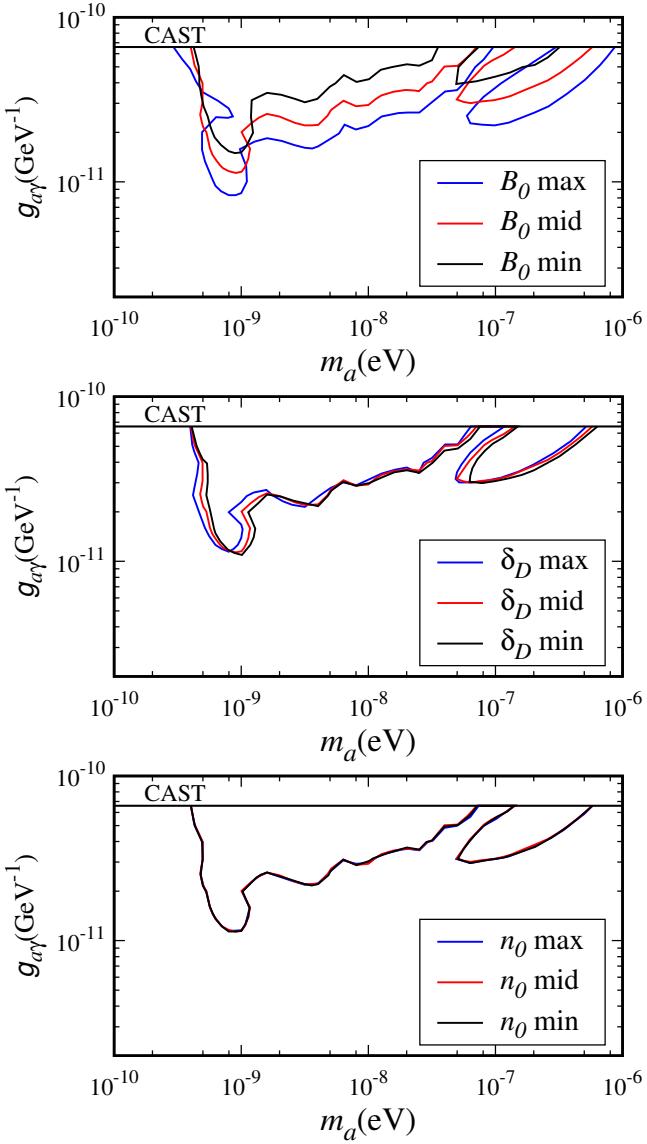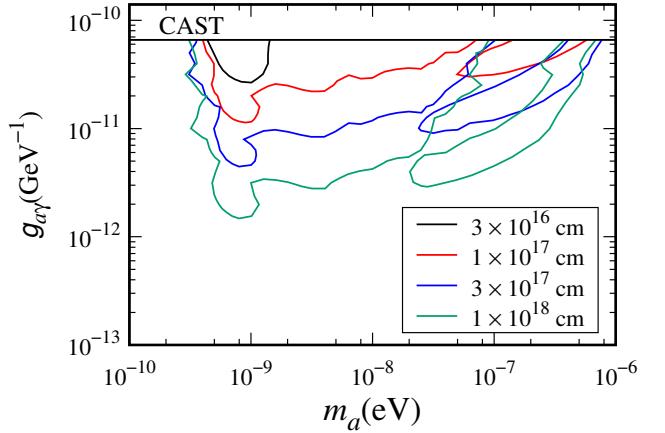FIG. 8. The combined constraints at 95% C.L. for the different values of r_{VHE}. The lines from top to bottom represent the results for four typical values of $r_{\mathrm{VHE}} = 3 \times 10^{16}$, 1×10^{17}, 3×10^{17}, and 1×10^{18} cm. The other parameters for the BJMF model are taken as the benchmark values listed in Table I.

TABLE IV. The modified values of the BJMF parameters in the ten phases used for Fig. 7.

Phase	$B_0(\mathrm{G})$		δ_{D}		$n_0(10^3 \mathrm{~cm}^{-3})$	
	min	max	min	max	min	max
S1	0.036	0.060	34	44	1.703	2.223
S2	0.12	0.24	13	19	2.404	3.878
OB	0.049	0.080	30	38	1.933	2.704
F1	0.10	0.21	8	12	0.013	3.381
F2	0.068	0.120	15	20	0.137	3.123
F3	0.063	0.091	38	46	1.092	1.939
F4	0.020	0.052	28	45	2.070	5.167
F5	0.025	0.180	18	52	1.024	4.728
F6	0.052	0.138	10	39	1.109	20.020
F7	0.083	0.153	25	37	1.326	3.077

VI. CONCLUSION

In this work, we investigate the ALP-photon oscillation effect in the spectra of the blazar Mrk 421 measured by ARGO-YBJ and *Fermi*-LAT during the common operation time, which cover ten activity phases of Mrk 421. We find that no significant ALP-photon oscillation effect is confirmed. However, only the observations of several phases can be individually used to set the constraint at 95% C.L. on the ALP parameter space.

The constraint on the ALP-photon coupling $g_{a\gamma}$ becomes stricter when the analyses for the data of the ten phases are combined. Compared with the limits set by the PKS 2155-304 observation of H.E.S.S. [48] and the NGC 1275 observation of *Fermi*-LAT [49], the upper limit on $g_{a\gamma}$ set by the ARGO-YBJ and *Fermi*-LAT observations of Mrk 421 is within $\sim [2 \times 10^{-11}, \ 6 \times$

FIG. 7. The combined constraints at 95% C.L. for the different values of B_0, δ_{D}, and n_0. In each panel, we only change one parameter and take other parameters as the benchmark values listed in Table I. For the parameters B_0, δ_{D}, and n_0, the 1σ values in the minimal and maximal cases are given by Table IV. The "mid" lines represent the result with the benchmark values of all parameters listed in Table I.

be larger than other parameters. Here we choose other three typical values of 3×10^{16}, 3×10^{17}, and 1×10^{18} cm for r_{VHE}. Since r_{VHE} directly characterizes the magnetic field strength and could significantly affects the ALP-photon oscillation effect, it can be seen that the large uncertainties of r_{VHE} significantly affect the final constraints.

10^{-11}] GeV^{-1} for the ALP mass of $\sim 5 \times 10^{-10}$ eV $\lesssim m_a \lesssim 5 \times 10^{-7}$ eV at 95% C.L.

We also show the impact of the BJMF parameters on the final constraints. We find that the final constraints are significantly affected by the magnetic field strength in the emission region B_0 and especially the distance of the emission region to the central black hole r_{VHE}. The constraints would become more accurate when further information about these parameters will be available.

In the future, the forthcoming VHE γ-ray observations, such as CTA [86] and LHAASO [87] will collect more data for the high energy γ-ray sources at large distances from the Earth with high precision. Using these results, it is possible to set the more stringent constraints on the ALP parameter space.

[1] R. Peccei and H. R. Quinn, Phys. Rev. D **16**, 1791 (1977).

[2] R. Peccei and H. R. Quinn, Phys. Rev. Lett. **38**, 1440 (1977).

[3] S. Weinberg, Phys. Rev. Lett. **40**, 223 (1978).

[4] F. Wilczek, Phys. Rev. Lett. **40**, 279 (1978).

[5] J. E. Kim, Phys. Rept. **150**, 1 (1987).

[6] P. Svrcek and E. Witten, JHEP **06**, 051 (2006), arXiv:hep-th/0605206.

[7] A. Arvanitaki, S. Dimopoulos, S. Dubovsky, N. Kaloper, and J. March-Russell, Phys. Rev. D **81**, 123530 (2010), arXiv:0905.4720 [hep-th].

[8] D. J. E. Marsh, Phys. Rept. **643**, 1 (2016), arXiv:1510.07633 [astro-ph.CO].

[9] J. Preskill, M. B. Wise, and F. Wilczek, Phys. Lett. B **120**, 127 (1983).

[10] L. Abbott and P. Sikivie, Phys. Lett. B **120**, 133 (1983).

[11] M. Dine and W. Fischler, Phys. Lett. B **120**, 137 (1983).

[12] M. Khlopov, A. Sakharov, and D. Sokoloff, Nucl. Phys. B Proc. Suppl. **72**, 105 (1999).

[13] P. Sikivie, Int. J. Mod. Phys. A **25**, 554 (2010), arXiv:0909.0949 [hep-ph].

[14] D. B. Kaplan, Nucl. Phys. B **260**, 215 (1985).

[15] P. Sikivie, Phys. Rev. Lett. **51**, 1415 (1983), [Erratum: Phys.Rev.Lett. 52, 695 (1984)].

[16] G. Raffelt and L. Stodolsky, Phys. Rev. D **37**, 1237 (1988).

[17] K. Zioutas et al., Nucl. Instrum. Meth. A **425**, 480 (1999), arXiv:astro-ph/9801176.

[18] V. Anastassopoulos et al. (CAST), Nature Phys. **13**, 584 (2017), arXiv:1705.02290 [hep-ex].

[19] E. Zavattini et al. (PVLAS), Phys. Rev. Lett. **96**, 110406 (2006), arXiv:hep-ex/0507107.

[20] M. Bregant et al. (PVLAS), Phys. Rev. D **78**, 032006 (2008), arXiv:0805.3036 [hep-ex].

[21] P. Pugnat et al. (OSQAR), Phys. Rev. D **78**, 092003 (2008), arXiv:0712.3362 [hep-ex].

[22] R. Ballou et al. (OSQAR), Phys. Rev. D **92**, 092002 (2015), arXiv:1506.08082 [hep-ex].

[23] Y. Kahn (ABRACADABRA), Springer Proc. Phys. **211**, 135 (2018).

[24] J. L. Ouellet et al., Phys. Rev. Lett. **122**, 121802 (2019), arXiv:1810.12257 [hep-ex].

[25] A. De Angelis, M. Roncadelli, and O. Mansutti, Phys. Rev. D **76**, 121301 (2007), arXiv:0707.4312 [astro-ph].

[26] D. Hooper and P. D. Serpico, Phys. Rev. Lett. **99**, 231102 (2007), arXiv:0706.3203 [hep-ph].

[27] M. Simet, D. Hooper, and P. D. Serpico, Phys. Rev. D **77**, 063001 (2008), arXiv:0712.2825 [astro-ph].

[28] A. V. Belikov, L. Goodenough, and D. Hooper, Phys. Rev. D **83**, 063005 (2011), arXiv:1007.4862 [astro-ph.HE].

[29] A. De Angelis, G. Galanti, and M. Roncadelli, Phys. Rev. D **84**, 105030 (2011), [Erratum: Phys.Rev.D 87, 109903 (2013)], arXiv:1106.1132 [astro-ph.HE].

[30] F. Tavecchio, M. Roncadelli, G. Galanti, and G. Bonnoli, Phys. Rev. D **86**, 085036 (2012), arXiv:1202.6529 [astro-ph.HE].

[31] F. Tavecchio, M. Roncadelli, and G. Galanti, Phys. Lett. B **744**, 375 (2015), arXiv:1406.2303 [astro-ph.HE].

[32] M. Meyer, D. Horns, and M. Raue, Phys. Rev. D **87**, 035027 (2013), arXiv:1302.1208 [astro-ph.HE].

[33] M. Meyer, D. Montanino, and J. Conrad, JCAP **09**, 003 (2014), arXiv:1406.5972 [astro-ph.HE].

[34] G. Galanti, M. Roncadelli, A. De Angelis, and G. F. Bignami, Mon. Not. Roy. Astron. Soc. **493**, 1553 (2020), arXiv:1503.04436 [astro-ph.HE].

[35] M. Meyer, M. Giannotti, A. Mirizzi, J. Conrad, and M. Sánchez-Conde, Phys. Rev. Lett. **118**, 011103 (2017), arXiv:1609.02350 [astro-ph.HE].

[36] J. Majumdar, F. Calore, and D. Horns, PoS **IFS2017**, 168 (2017), arXiv:1711.08723 [hep-ph].

[37] G. Galanti and M. Roncadelli, Phys. Rev. D **98**, 043018 (2018), arXiv:1804.09443 [astro-ph.HE].

[38] G. Galanti and M. Roncadelli, JHEAp **20**, 1 (2018), arXiv:1805.12055 [astro-ph.HE].

[39] G. Galanti, F. Tavecchio, M. Roncadelli, and C. Evoli, Mon. Not. Roy. Astron. Soc. **487**, 123 (2019), arXiv:1811.03548 [astro-ph.HE].

[40] B. Berenji, J. Gaskins, and M. Meyer, Phys. Rev. D **93**, 045019 (2016), arXiv:1602.00091 [astro-ph.HE].

[41] R. Reesman and T. Walker, JCAP **08**, 021 (2014), arXiv:1402.2533 [astro-ph.HE].

[42] C. Zhang, Y.-F. Liang, S. Li, N.-H. Liao, L. Feng, Q. Yuan, Y.-Z. Fan, and Z.-Z. Ren, Phys. Rev. D **97**, 063009 (2018), arXiv:1802.08420 [hep-ph].

[43] Y.-F. Liang, C. Zhang, Z.-Q. Xia, L. Feng, Q. Yuan, and Y.-Z. Fan, JCAP **06**, 042 (2019), arXiv:1804.07186 [hep-ph].

[44] G. Long, W. Lin, P. Tam, and W. Zhu, Phys. Rev. D **101**, 063004 (2020), arXiv:1912.05309 [astro-ph.HE].

[45] K. Kohri and H. Kodama, Phys. Rev. D **96**, 051701 (2017), arXiv:1704.05189 [hep-ph].

[46] M. Libanov and S. Troitsky, Phys. Lett. B **802**, 135252 (2020), arXiv:1908.03084 [astro-ph.HE].

[47] X.-J. Bi, Y. Gao, J. Guo, N. Houston, T. Li, F. Xu, and X. Zhang, Phys. Rev. D **103**, 043018 (2021), arXiv:2002.01796 [astro-ph.HE].

[48] A. Abramowski et al. (H.E.S.S.), Phys. Rev. D **88**, 102003 (2013), arXiv:1311.3148 [astro-ph.HE].

[49] M. Ajello et al. (Fermi-LAT), Phys. Rev. Lett. **116**, 161101 (2016), arXiv:1603.06978 [astro-ph.HE].

[50] J. Guo, H.-J. Li, X.-J. Bi, S.-J. Lin, and P.-F. Yin, Chin. Phys. C **45**, 025105 (2021), arXiv:2002.07571 [astro-ph.HE].

[51] G. A. Pallathadka, F. Calore, P. Carenza, M. Giannotti, D. Horns, J. Majumdar, A. Mirizzi, A. Ringwald, A. Sokolov, and F. Stief, (2020), arXiv:2008.08100 [hep-ph].

[52] M. Punch et al., Nature **358**, 477 (1992).

[53] F. Aharonian et al. (HEGRA), Astron. Astrophys. **393**, 89 (2002), arXiv:astro-ph/0205499.

[54] F. Aharonian et al. (H.E.S.S.), Astron. Astrophys. **437**, 95 (2005), arXiv:astro-ph/0506319.

[55] J. Albert et al. (MAGIC), Astrophys. J. **663**, 125 (2007), arXiv:astro-ph/0603478.

[56] V. A. Acciari et al. (MAGIC, VERITAS), Astrophys. J. **703**, 169 (2009), arXiv:0907.3923 [astro-ph.HE].

[57] A. A. Abdo et al. (LAT, MAGIC), Astrophys. J. **736**, 131 (2011), arXiv:1106.1348 [astro-ph.HE].

[58] B. Bartoli et al. (ARGO-YBJ), Astrophys. J. **734**, 110 (2011), arXiv:1106.0896 [astro-ph.HE].

[59] B. Bartoli et al. (ARGO-YBJ), Astrophys. J. Suppl. **222**, 6 (2016), arXiv:1511.06851 [astro-ph.HE].

[60] V. A. Acciari et al. (MAGIC), Mon. Not. Roy. Astron. Soc. **486**, 4233 (2019), arXiv:1904.00134 [astro-ph.HE].

[61] A. Abdo et al., Astrophys. J. **716**, 30 (2010), arXiv:0912.2040 [astro-ph.CO].

[62] M. C. Begelman, R. D. Blandford, and M. J. Rees, Rev. Mod. Phys. **56**, 255 (1984).

[63] G. Ghisellini and F. Tavecchio, Mon. Not. Roy. Astron. Soc. **397**, 985 (2009), arXiv:0902.0793 [astro-ph.CO].

[64] R. Pudritz, M. Hardcastle, and D. Gabuzda, Space Sci. Rev. **169**, 27 (2012), arXiv:1205.2073 [astro-ph.HE].

[65] S. P. O'Sullivan and D. C. Gabuzda, Mon. Not. Roy. Astron. Soc. **400**, 26 (2009), arXiv:0907.5211 [astro-ph.CO].

[66] O. Hervet, D. A. Williams, A. D. Falcone, and A. Kaur, Astrophys. J. **877**, 26 (2019), arXiv:1904.06802 [astro-ph.HE].

[67] B. Banerjee, M. Joshi, P. Majumdar, K. E. Williamson, S. G. Jorstad, and A. P. Marscher, Mon. Not. Roy. Astron. Soc. **487**, 845 (2019), arXiv:1905.01043 [astro-ph.GA].

[68] A. Celotti and G. Ghisellini, Mon. Not. Roy. Astron. Soc. **385**, 283 (2008), arXiv:0711.4112 [astro-ph].

[69] C. Carilli and G. Taylor, Ann. Rev. Astron. Astrophys. **40**, 319 (2002), arXiv:astro-ph/0110655.

[70] F. Govoni and L. Feretti, Int. J. Mod. Phys. D **13**, 1549 (2004), arXiv:astro-ph/0410182.

[71] K. Subramanian, A. Shukurov, and N. E. L. Haugen, Mon. Not. Roy. Astron. Soc. **366**, 1437 (2006), arXiv:astro-ph/0505144.

[72] M. Pshirkov, P. Tinyakov, and F. Urban, Phys. Rev. Lett. **116**, 191302 (2016), arXiv:1504.06546 [astro-ph.CO].

[73] P. Ade et al. (Planck), Astron. Astrophys. **594**, A19 (2016), arXiv:1502.01594 [astro-ph.CO].

[74] A. Franceschini, G. Rodighiero, and M. Vaccari, Astron. Astrophys. **487**, 837 (2008), arXiv:0805.1841 [astro-ph].

[75] P. Madau and L. Pozzetti, Mon. Not. Roy. Astron. Soc. **312**, L9 (2000), arXiv:astro-ph/9907315.

[76] G. Fazio et al. (IRAC), Astrophys. J. Suppl. **154**, 10 (2004), arXiv:astro-ph/0405616.

[77] D. Elbaz, C. Cesarsky, P. Chanial, H. Aussel, A. Franceschini, D. Fadda, and R. Chary, Astron. Astrophys. **384**, 848 (2002), arXiv:astro-ph/0201328.

[78] C. Papovich et al., Astrophys. J. Suppl. **154**, 70 (2004), arXiv:astro-ph/0406035.

[79] G. Lagache, L. Haffner, R. Reynolds, and S. Tufte, Astron. Astrophys. **354**, 247 (2000), arXiv:astro-ph/9911355.

[80] R. Jansson and G. R. Farrar, Astrophys. J. Lett. **761**, L11 (2012), arXiv:1210.7820 [astro-ph.GA].

[81] B. Bartoli et al., Phys. Rev. D **84**, 022003 (2011), arXiv:1107.4887 [astro-ph.HE].

[82] W. Atwood et al. (Fermi-LAT), Astrophys. J. **697**, 1071 (2009), arXiv:0902.1089 [astro-ph.IM].

[83] B. Bartoli et al., The Astronomer's Telegram **4272**, 1 (2012).

[84] F. D'Ammando and M. Orienti, The Astronomer's Telegram **4261**, 1 (2012).

[85] B. Bartoli et al. (ARGO-YBJ), Astrophys. J. **779**, 27 (2013), arXiv:1311.3376 [astro-ph.HE].

[86] B. Acharya et al. (CTA Consortium), Astropart. Phys. **43**, 3 (2013).

[87] Z. Cao (LHAASO), Chin. Phys. C **34**, 249 (2010).